(4) Numerical simulations have been carried out to clarify the meaning of API recommendation on the ratio of coarse grained zone occupied along the crack front. Present analytical results are consistent with the experimental tendency obtained by others and show the API recommendation of 15 percent on the coarse grained zone ratio to whole length of the crack front is not always conservative to get eventual low CTOD value.
(5) The effect of specimen thickness on the CTOD values of HAZ was also investigated using the statistical model taking also into account of the mechanical constraint effect. It was shown that in case of HAZ CTOD, plate thickness effect was controlled primarily by the metallurgical effect.

Acknowledgements

The present work is one of several attempts to interpret the experimental data generated by the FTW Committee of the Japan Welding Engineering Society (JWES), the main purpose of which is to draft recommendations for CTOD testing on weldments. The authors wish to extend their sincere gratitude for the Committee members' valuable discussion as well as their great assistance in carrying out the tedious experiments, particularly to Professor Toyoda and Dr Minami (Osaka University), Professor Toyosada (Kyushu University), five leading Japanese Steel manufacturers, Mitsubishi Heavy Industries Ltd, and other fabricators. The authors also express their appreciation to Dr Aihara of Nippon Steel Corporation for his useful suggestions for drafting this paper.

References

(1) *API Recommended Practice* **2Z(RP2Z)**, (1987).
(2) *Steel Specification for Offshore Structures* (EEMUA **150**), (1987).
(3) FAIRCHILD, D. P., THEISEN, J. D., and ROYER, C. P. (1988) *Proc. Int. Conf. Offshore Mech. and Arctic Engng*, ASME, Vol. **3**, p. 247.
(4) MACHIDA, S., MIYATA, T., TOYOSADA, M., and HAGIWARA, Y. Proc. symp. on fatigue and fracture testing of weldments, *ASTM STP* **1058**, 1988.
(5) PALEY, Z., LYNCH, J. N., and ADAMS, C. M. (1964) *Welding J.*, **43**, 2.
(6) HAZE, T. and AIHARA, S. (1986) IIW Doc. IX–1423–86, Tokyo.
(7) SATOH, K., TOYODA, M., and MINAMI, F. (1985) *Trans. Japan Welding Soc.*, **16**, 70.
(8) HAZE, T. and AIHARA, S. (1989) *Proc. 7th Int. Conf. Offshore Mech. and Arctic Engng*, ASME, Vol. **III**, p. 515.
(9) FAIRCHILD, D. P., Proc. symp. on fatigue and fracture testing of weldments, *ASTM STP* **2058**, 1988.
(10) KAWANO, S. (1984) *Fundamental study on plate thickness effect on fracture toughness of structural steels under large-scale yielding condition*, PhD thesis, Hiroshima University (in Japanese).

J. Heerens, D. T. Read†, A. Cornec*, and K.-H. Schwalbe**

Interpretation of Fracture Toughness in the Ductile-to-Brittle Transition Region by Fractographical Observations

REFERENCE Heerens, J., Read, D. T., Cornec, A., and Schwalbe, K.-H., **Interpretation of fracture toughness in the ductile-to-brittle transition region by fractographical observations**, *Defect Assessment in Components – Fundamentals and Applications*, ESIS/EGF9 (Edited by J. G. Blauel and K.-H. Schwalbe) 1991, Mechanical Engineering Publications, London, pp. 659–678.

ABSTRACT The reason for the scatter of fracture toughness in the ductile-to-brittle transition region has been investigated for the quenched and tempered pressure vessel steel 20MnMoNi55. Fractographic results confirm the weakest-link mechanism of cleavage initiation. Four different types of initiation sites could be classified. The initiation sites of cleavage fracture are located at the peak of the normal stress in front of the fatigue crack tip. One conclusion of this paper indicates that a large part of the scatter of the fracture toughness results from the scatter of the distance between the initiation site and the fatigue crack tip. An estimation of the transition temperature using the cleavage fracture criterion postulated by Ritchie *et al.* is in agreement with the measured toughness values. The results lead to the conclusion that the J integral is not an appropriate parameter to give a specimen size independent characterization of cleavage fracture.

Introduction

For the characterization of the ductile-to-brittle transition behaviour of a steel, the transition curve is normally determined by measuring the fracture toughness as a function of temperature using small pre-cracked laboratory specimens. With the determination of the transition curve, the following problems generally arise.

- The fracture toughness (for the initiation of cleavage fracture) in the transition region exhibits high scatter, which increases with increasing temperature. The scatter becomes very large in the upper transition region; that is, the region where cleavage fracture is preceded by ductile tearing. Because of the large scatter, many specimens must be tested in order to get a reliable characterization of the material.
- The transition curve frequently depends on the size and geometry of the specimen, as well as on the loading rate used in the fracture test. As a consequence the test results measured on laboratory specimens are not directly applicable to cracks in a structure, which may have a different constraint or loading rate compared to the small specimen.

* Institut für Werkstofforschung, GKSS-Forschungszentrum Geesthacht GmbH, 2054 Geesthacht, FRG.
† Fracture and Deformation Division, National Institute of Standards and Technology, Boulder, CO, USA.

In order to avoid extensive testing within the transition region various statistical models have been developed which are aimed at predicting the scatterband as well as the size effects from a relatively small set of test data (1)(2). The models seem to work well when cleavage fracture occurs at small scale yielding during crack tip blunting. If cleavage fracture occurs after substantial plasticity of the ligament or after initiation of ductile tearing, the models generally seem to fail. More research is obviously necessary, which may lead to a better understanding of how ductile tearing and plastic deformation of the ligament influence cleavage fracture.

In this paper the reason for the scatter of fracture toughness in the upper transition region is investigated; this is the temperature region where cleavage fracture is preceded by some ductile tearing. The mechanisms triggering cleavage will be discussed. The cleavage fracture criterion of Ritchie *et al.* (3) will be used to estimate the transition temperature. Based on both the fractographic observations and some finite element solutions taken from the literature, the cleavage fracture behaviour of CCT (centre crack tension) and ECB (edge crack bending) specimens will be discussed.

Material

The material used in this study was DIN 20MnMoNi55 steel from a forged boiler bottom segment. The chemical composition of this steel is similar to A533B; see Table 1. The heat treatment of the material is shown in Fig. 1. All specimens were machined from 25 mm thick slices taken from one heat-treated block. The orientation of the fracture surfaces was the same for all types of specimens.

Experimental details

The specimens used in this study are shown in Fig. 2. For the determination of the fracture toughness, pre-cracked side grooved CT specimens were used. All specimens were pre-cracked at room temperature with a load ratio of $P_{min}/P_{max} = 0.1$. The K_{max} value for the final 1–2 mm of pre-cracking was about 500–700 N/mm$^{3/2}$. All specimens were 20 percent side grooved after pre-cracking. The J-integral was calculated according to ASTM E 813-81 (4) using the analysis for the multiple specimen technique.

Table 1 Composition of 20MnMoNi55 in weight percent

C	Si	Mn	P	S	Cr	V
0.19	0.2	1.29	0.007	0.008	0.12	0.02
Cu	Al	Ni	Mo	Sn	Co	As
0.11	0.015	0.8	0.53	0.012	0.014	0.03
Sb	Ti	Fe				
0.03	0.05	bal				

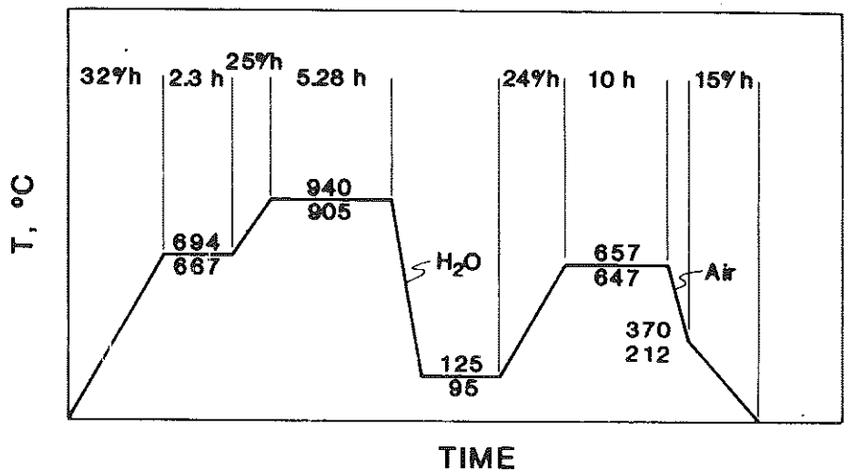

Fig 1 Heat treatment of the forged material

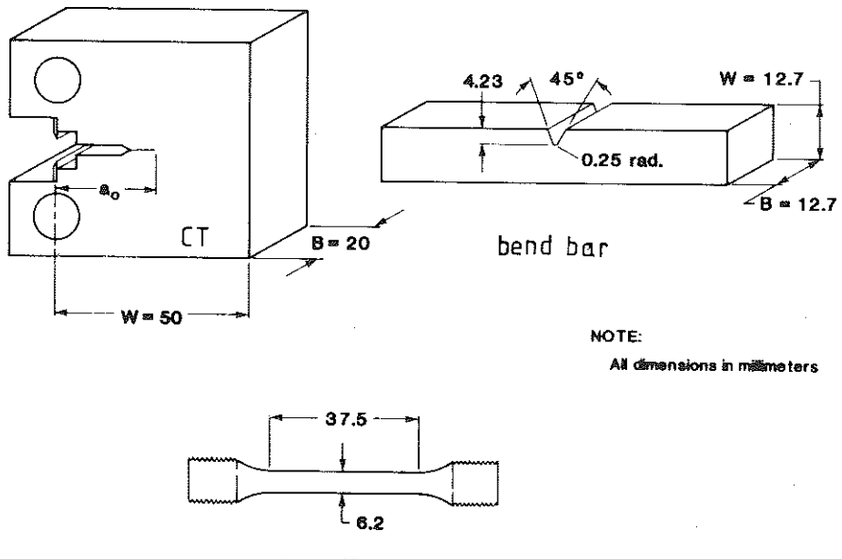

Fig 2 CT-specimens, blunt notched bend bars and tensile specimens used in this study

The blunt-notched specimens were machined and tested in four-point bending as shown in the reference (5).

The displacement (crosshead) rate was 0.5 mm/min for the CT specimens and for the bend bars. The tensile specimens were tested with a displacement rate of 1 mm/min.

For cooling the specimens, a bath of ethanol cooled with liquid nitrogen or a bath of pure liquid nitrogen was used, depending on the test temperature. In either case, the temperature was monitored by a thermocouple attached to the surface of the specimen or located within a small hole in the specimen. For qualitiative analysis of the inclusions, an energy dispersive analyser combined with a scanning electron microscope (SEM) was used.

Results

Fracture behaviour of the various specimens

CT specimens

A total of 30 specimens was tested in the temperature range of −45°C to −90°C. All specimens failed by cleavage fracture. For each specimen the critical J value, J_c, for cleavage fracture was calculated according to the reference (4).

In order to determine the scatter-band of J_c in this temperature range, a number of specimens was tested at −60°C and −90°C, respectively. The resulting data, Fig. 3, show that the scatter in J_c significantly increases with increasing temperature. In the diagram J_i indicates the initiation of ductile tearing. This J_i level was determined at −60 and −90°C by fractographic investigation of the fracture surface. At J_i, dimples first appear at the blunted crack tip.

Blunt notched bend bars

The finite element solutions of reference (5) are only valid for loads below net section yielding. For this reason all bend bar tests were conducted at the relatively low temperature of −196°C. At this temperature all tested specimens failed by cleavage fracture below the limit load.

Tensile specimens

The lower yield strength, R_{el}, and the ultimate tensile strength, R_m, were measured as a function of temperature, Fig. 4(a). Because of the assumption that the yield strength of the material is an important parameter for the cleavage fracture behaviour of the material, the scatter of the yield strength was measured carefully at temperatures where the ductile-to-brittle transition of the CT specimens occurs, Fig. 4(b).

At temperatures below −178°C all tensile specimens failed by cleavage fracture; at higher temperatures they failed by ductile tearing. At −196°C cleavage fracture of the specimens occurred without, or with little, necking of the specimens.

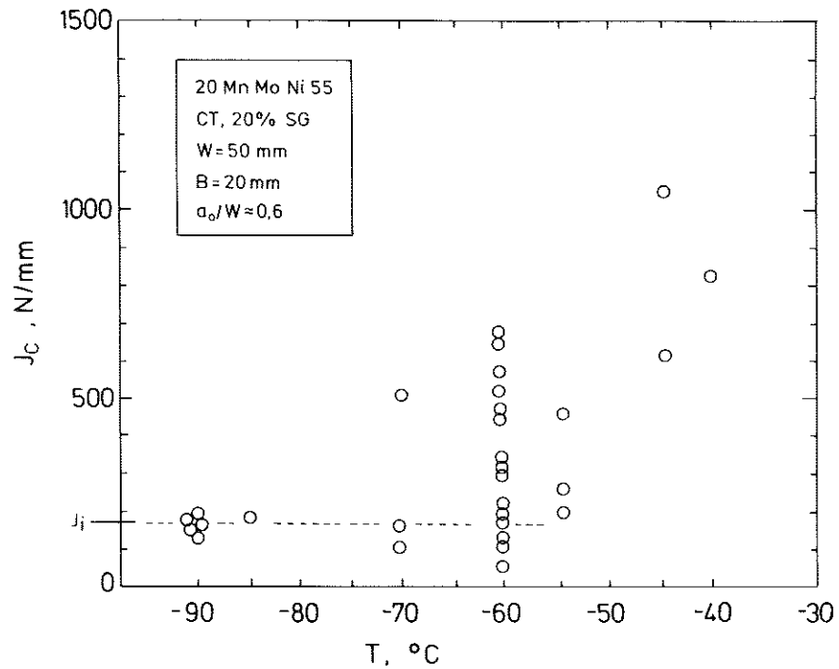

Fig 3 Fracture toughness, J_c, of the material in the upper transition region

Fractographic examination

The fracture surfaces of the specimens were investigated using a SEM. The objective was to find evidence for the microstructural mechanisms leading to cleavage fracture.

At low magnification, the fracture surfaces of each type of specimen exhibited macroscopic river patterns which originate at one small area on the fracture surface, see Fig. 5(a). Examinations of the centre of the macroscopic river patterns at high magnifications revealed fine river patterns. In all specimens, these river patterns could be traced to a single area which contains one cleavage facet, or sometimes a few. These areas are referred to as initiation sites. Four types of initiation sites were found by SEM examination.

Type F (facets)

One or sometimes a few cleavage facets are arranged at the initiation site. The size of the facets is about 50 to 90 μm, Fig. 5(b). No particles can be observed at the initiation site. This type appears mainly at low temperatures because in all the CT specimens tested at −90°C as well as in all bend bars tested at −196°C this type was found.

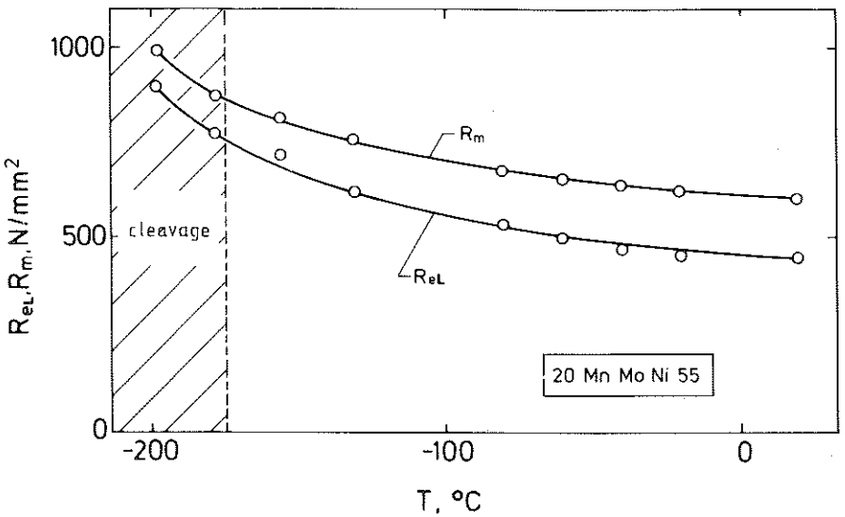

Fig 4(a) Tensile strength, R_m, and lower yield strength, R_{el}, versus temperature

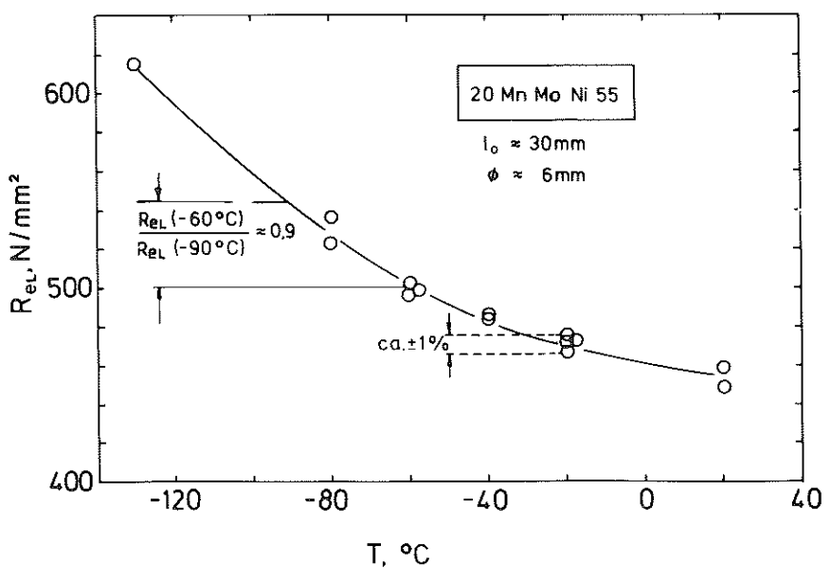

Fig 4(b) Scatter of the lower yield strength, R_{el}, within the transition regime of the CT specimens

Type I (inclusion)

Features similar to type F but one large inclusion or a few small inclusions are located on the facet. Fig. 5(c). The size of the inclusions ranged from 2 to 8 μm.

Type K (cluster)

In two of 26 CT specimens and in all tensile specimens tested at −196°C a cluster of large inclusions was found at the centre of the river pattern, see Fig. 5(d). The energy dispersive analysis of the various inclusions show mainly the elements Mn and S and traces of Si, Ti and Cu. This indicates manganese sulphide inclusions.

Type L (local tearing)

For J_c values higher than J_i, the specimens had ductile tearing along the crack front followed by cleavage fracture. In many of these specimens the initiation site is located close to a local ductile tearing zone. This zone is always connected with the main crack, see Fig. 5(e).

Location of initiation sites

The centre of the river pattern was assumed to be the cleavage initiation site. For all CT specimens and blunt-notched bend bars the location of the initiation site was determined. The distance, r_c, between the initiation site and the fatigue crack tip was measured; this distance does not include the stretched zone. In addition, the distance between the centreline of the specimen and the initiation sites was measured; this distance is designated as z. The results of these measurements and the results of the fractographic examinations are shown in Fig. 6 and Table 2. In Fig. 6 it can be seen that with increasing temperature the distance between the initiation site and the fatigue crack tip increases.

Discussion

Fracture stress in various specimens

Many investigations on cleavage fracture **(5)–(9)** have shown that the normal stresses in a material have a good correlation with the cleavage fracture behaviour of the material. This is based on the assumption that Griffith-cracks exist in the material which become unstable if a critical normal stress level is reached.

The fact that the cleavage initiation sites can be localized in all tested specimens provides the opportunity to investigate this assumption. In the following section the correlation between the normal stress in the ligament and cleavage fracture is considered.

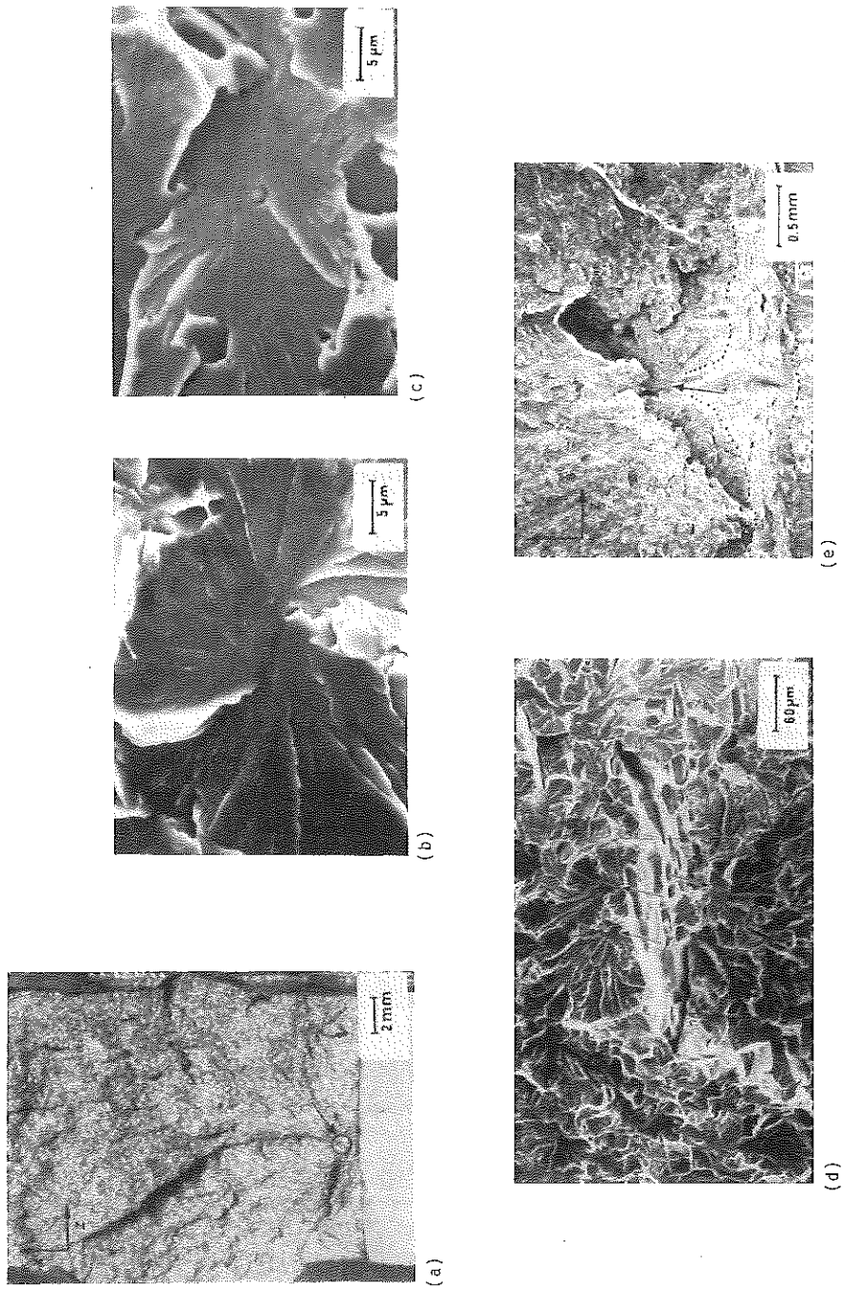

CT specimens

It has been shown by finite element calculations **(10)–(12)** and by the slip line theory **(13)** that for a blunted crack the normal stresses σ_y have a maximum at a certain distance ahead of the crack tip, see Fig. 7. The solutions shown in Fig. 7 are based on a power law hardening material, N is the strain hardening exponent and σ_0 the yield strength of the material.

The location and magnitude of the stress maximum depends on the strain hardening and slightly on the ratio of yield strength to Young's modulus. At the test temperatures, the material used in this study has a strain hardening exponent N of about 0.1 (see explanations below) and the ratio σ_0/E is about 0.0025 as it is assumed in Fig. 7. Therefore, as an approximation according to Fig. 7 the maximum of σ_y for the material used in this study is assumed to be located at the normalized distance of $A = A_m = 0.0027$. (Figure 7 does not directly support the choice of 0.0027 but later it will be shown that the σ_y stress peak seems to control cleavage fracture of the specimen and the choice of 0.0027 is needed to calculate a transition temperature which is in agreement with the experimental results.) The normalized distance is defined as

$$A = \frac{r\sigma_0^2(1-\nu^2)}{EJ} \tag{1}$$

For a sharp crack, Schwalbe **(14)** has derived an analytical solution for σ_y which is in agreement with these finite element solutions for the distances $A > A_m$, that is the range beyond the maximum of the stress peak. In order to estimate the normal stress distribution in the ligament of the CT specimens the results from the literature will be used as follows: For the range at and beyond the maximum which is characterized by $A > A_m = 0.0027$ Schwalbe's solution was used

$$\sigma_y = \left\{\frac{0.3}{A+0.1}\left(\frac{0.04}{A}\right)^{N/N+1}\right\} \cdot \sigma_0 \tag{2}$$

For the range $A < A_m$ Schwalbe's solution leads to an over-estimation of the normal stresses because it does not account for crack tip blunting. In order to get a reasonable estimation of the normal stresses the shape of the slip line solution **(13)** was adopted within that range.

(*see facing page*)

Fig 5 (a) Fracture surface of a CT specimen showing macroscopic river pattern which emanates from one small area on the fracture surface in front of the fatigue crack tip (b)–(e) Different types of cleavage initiation sites: (b) Type F: a cleavage facet is located at the centre of the river pattern; (c) Type I: an inclusion is located at the centre of the river pattern; (d) Type K: a cluster of large inclusions in the centre of the coarse river pattern; a number of single cleavage initiation sites form the centre of the fine river pattern at the border of the cluster; (e) Type L: cleavage fracture initiation at a local zone of ductile tearing

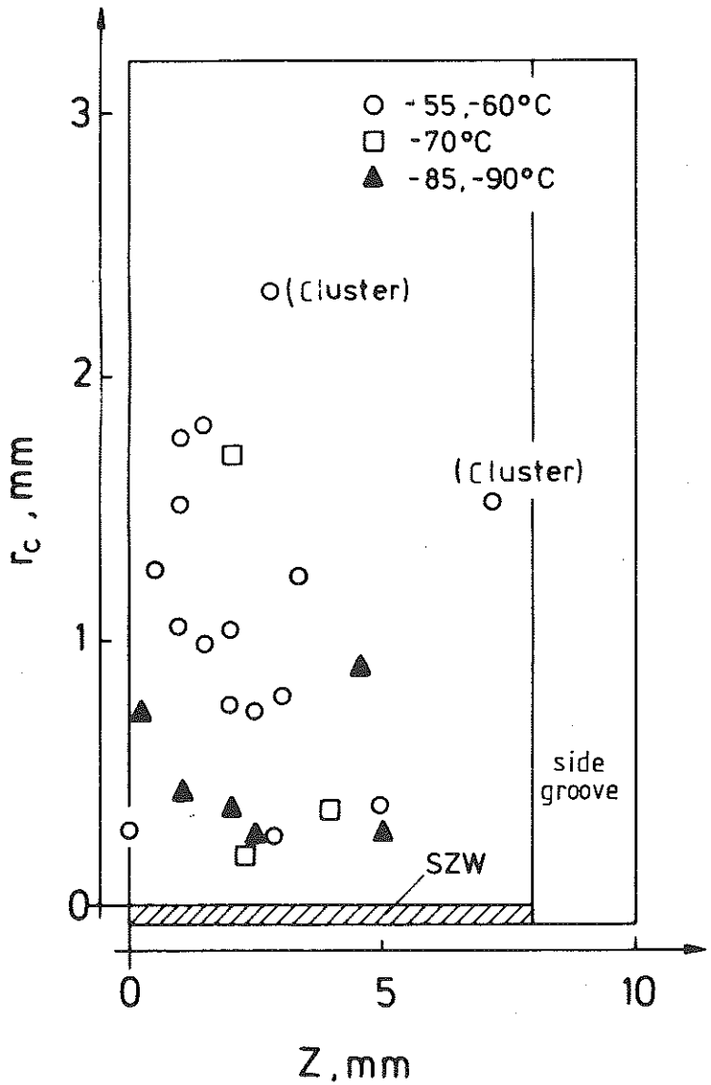

Fig 6 Location of the initiation sites in the ligament. The location of initiation sites depends on the test temperature

The hardening exponent N of the material was determined by fitting a power law through the true stress–strain curve of the uniaxial tensile data. For this purpose the true stress and true total strains were plotted on logarithmic axis. N was then determined by taking the slope of a straight line which was pinned at the following two points: the true stress referring to the maximum load and the yield point $R_{p0.2}$. This method of fitting the stress–strain curve is outlined in detail in reference **(15)**. Within the temperature range used in this study (−90 to −50°C) this procedure gives a hardening exponent of $N = 0.1$ which is only slightly influenced by the temperature. As an estimation of σ_0 the lower yield strength of the material, R_{el}, was adopted for the calculations.

Table 2 Fractographic results

Specimen number	J_c (*N/mm*)	T (°C)	*Initiation type*	r_c (*mm*)	z (*mm*)	σ_c (*N/mm*)
CT specimens						
EP7	184	−90	F	0.4	1	1988
EP10	180	−90	F	0.27	2.5	1924
EP1	170	−90	F	0.3	2.2	1970
EP6	157	−90	F	0.28	5.0	1970
EL11	124	−90	F	0.9	4.5	1700
EL12	180	−85	I	0.77	0.3	1822
EL4	100	−70	F	0.16	2.2	1800
EM6	150	−70	I	0.34	3	1900
EL3	500	−70	I	1.68	2.3	1825
EP12	60	−60	I	0.25	0	1750
EP8	120	−60	K	1.49	6.5	1450
EQ3	124	−60	I	0.21	3.0	1800
EP4	168	−60	F	0.48	0.5	1822
EL7	195	−60	I	0.74	2.1	1744
EP9	215	−60	I	1.08	2	1716
EQ4	286	−60	F	0.7	2.5	1866
EP2	304	−60	F	0.96	1.5	1808
EQ2	340	−60	L	0.8	3	1830
EP14	434	−60	L	1.28	1.2	1866
EP15	448	−60	L	1.76	1	1760
EP3	518	−60	L	1.23	0.5	1860
EQ1	560	−60	L	1.78	1.5	1805
EI16	630	−60	F	1.48	1.1	1855
EP11	190	−55	F	0.31	5	1755
EL10	250	−55	K	2.3	2.7	1560
EL5	455	−55	F	1.3	3.4	1817
Bend bars						
22		−196	F	0.59		1980
23		−196	F	0.33		1950
25		−196	F	0.28		1750
24		−196	F	0.21		1665

Using this approach, the fracture stress σ_c for each CT specimen was calculated using equation (2) by introducing r_c, the lower yield strength R_{el} and the hardening exponent of $N = 0.1$. The fracture stress values are tabulated in Table 2.

In Fig. 8 the location of the cleavage initiation sites of the CT specimens in relation to the normal stress distribution is shown. It can be seen that the initiation sites are located close to the normal stress peak. In addition the distribution of the initiation sites has a shape very similar to the shape of the stress distribution.

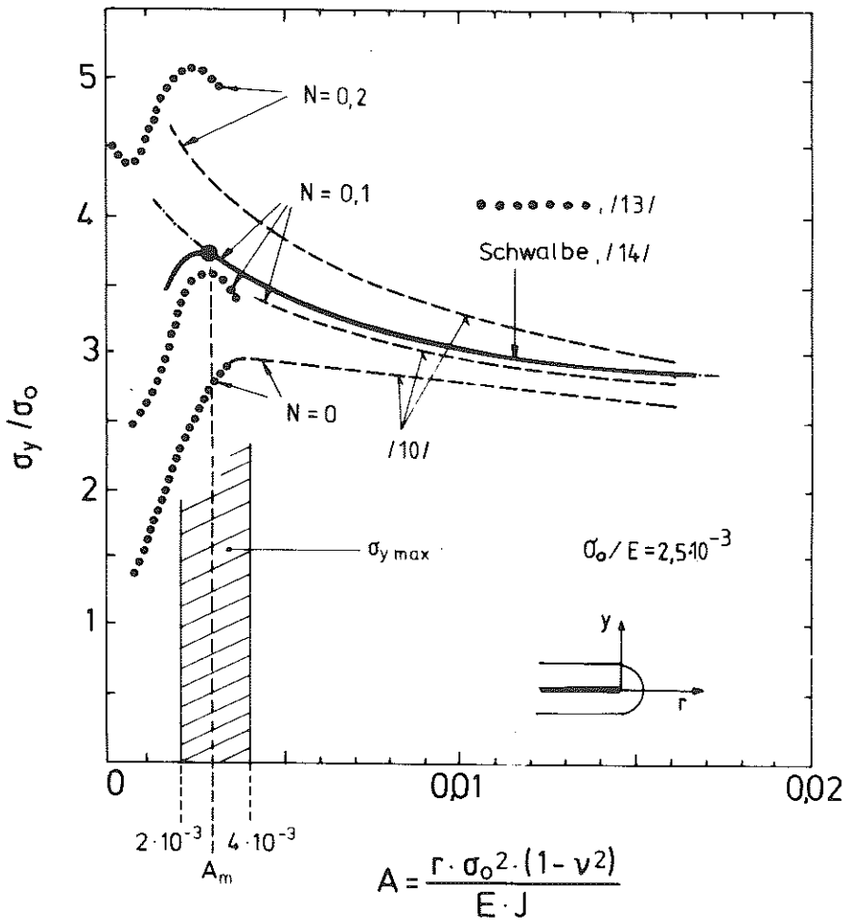

Fig 7 Normal stress σ_y in front of the blunted crack tip. The maximum was assumed to be at $A_m = 0.0027$. For the estimation of σ_y in front of the maximum, for $A > A_m$, Schwalbe's solution (14) was used. For the range $A < A_m$ the shape of the slip line solution (13) was adopted

Blunt-notched bend bars

For the notched bend bars the fracture stress σ_c was calculated using the small scale yielding finite element solution given in **(5)**. In these numerical calculations the normal stress is only available for discrete numbers of loading steps. In order to get the normal stress distribution for the actual failure loads of the bend bars, the numerical results were interpolated (dotted lines in Fig. 9). For four specimens the fracture stress was then estimated by determining the normal stress at the location of the initiation site as shown in Fig. 9 (see

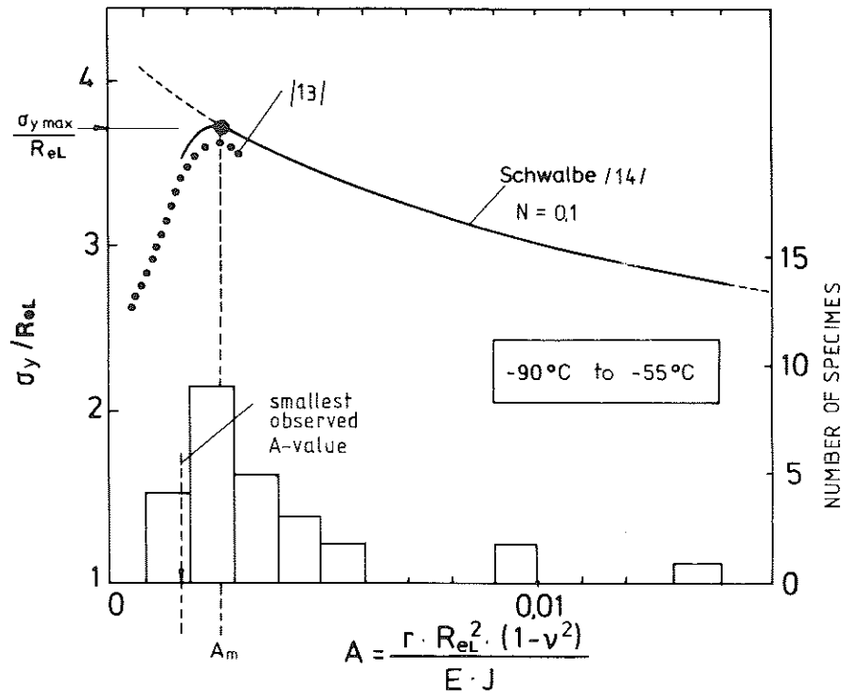

Fig 8 Location of the initiation sites of the CT specimens in relation to the normal stress σ_y

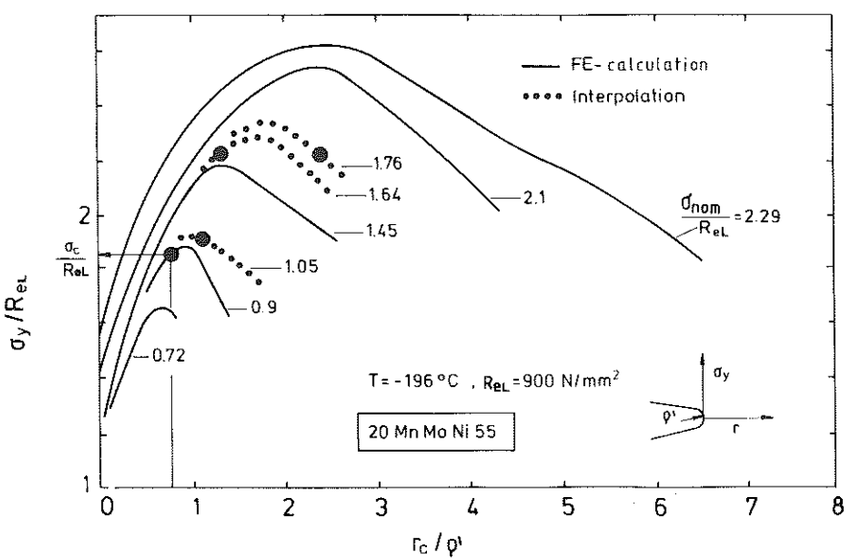

Fig 9 Location of the initiation sites of the blunt notched bend bars in relation to the normal stress σ_y

Table 2). Also in this type of specimen initiation of cleavage fracture occurs close to the maximum of the normal stress.

Tensile specimen

At −196°C cleavage fracture of the tensile specimens occurred without significant necking. Therefore, the stresses in the specimens were considered to be uniaxial. Using this approach the fracture stress was determined by

$$\sigma_c = \frac{F_c}{S}$$

F_c is the failure load of the specimen and S indicates the area of the cleavage fracture surface. In Fig. 10, the fracture stresses of the various types of specimen at various temperatures are summarized. Figure 10 reveals the following facts:

- Different types of specimens have approximately the same fracture stress.
- Concerning the calculated critical stress, the data in Fig. 10 can be divided in two groups, A and B. Group A is created by the initiation types F, I, L (facet, inclusion, local tearing). Group B is formed by the initiation type K (cluster). Compared to initiation types F, I, L the cluster have significantly lower fracture stresses. Each data group seems to have its own 'lower bound fracture stress' that is σ_A and σ_B. Below these stress levels the initiation of cleavage fracture seems to be very unlikely.
- For each group there is no significant influence of temperature on the 'lower bound fracture stress'.

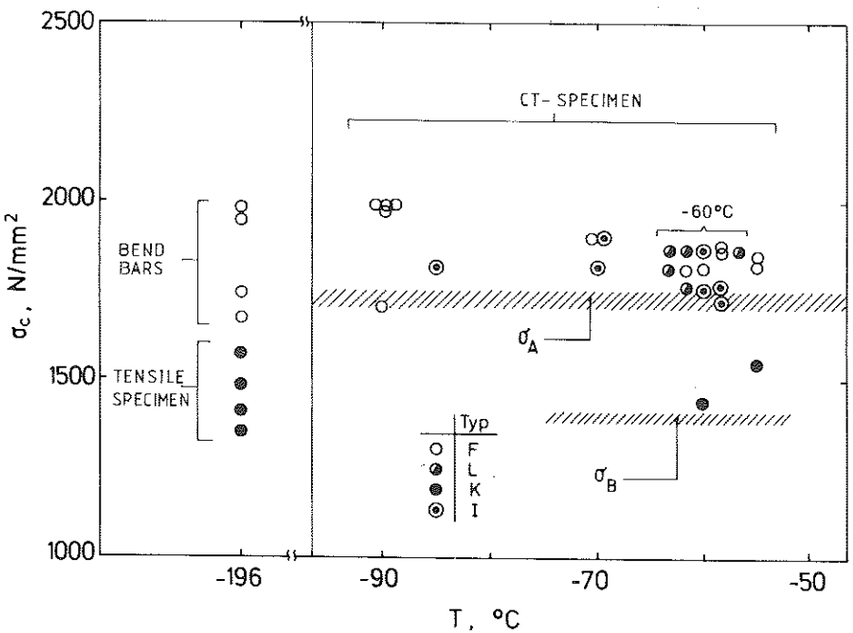

Fig 10 Fracture stress of the various specimens for the various types of specimens

The fact that a lower bound of fracture stress seems to exist in the material is in agreement with the cleavage fracture criterion postulated by Ritchie *et al.* **(3).**

Scatter of the fracture toughness

Figure 11(a) and 11(b) plots the J_c values versus r_c values for the CT specimens tested at −90 and −60°C, respectively. Two lines indicate the range in which the normal stresses in front of the crack tip is about 90 percent of the maximum-normal stress value σ_{ymax}. This range is approximately determined by $0.002 < A < 0.004$. Most of the r_c–J_c data points fall into this range; only a few are located slightly in front of the stress maximum.

These results show that the scatter of J_c values is essentially controlled by r_c, the distance between the cleavage initiation site and the fatigue crack tip. The distance r_c obviously characterizes how far the normal stress peak must move into the ligament in order to find the cleavage initiation site.

Some aspects of the lower bound fracture toughness and the transition temperature

The approach discussed above does not explain the existence of a lower bound fracture toughness. In principle, a cleavage initiation site may be located very close to the fatigue crack tip. Considering the correlation between r_c and J_c, this would lead to a vanishing J_c as r_c approaches zero. In all tests conducted in this study, no r_c values smaller than 210 μm have been found. This indicates that the initiation of cleavage fracture close to the crack tip is very unlikely. An interpretation of these results can be made by the RKR fracture criterion which postulates that cleavage fracture can only occur if the fracture stress is reached or exceeded over a critical distance. Due to the relationship between J and the shape of the normal-stress peak, the RKR fracture criterion can only be satisfied when J is large enough to provide a normal 'stress-peak-width' larger than the critical distance. Because with increasing J the peak moves away from the crack tip, the condition of having a stress peak of sufficient width is only possible at a certain distance in front of the crack tip. This means that the initiation sites must always be located at a certain distance in front of the fatigue crack tip. The experimental findings seem to support this model which is able to explain the existence of a lower bound fracture toughness.

The magnitude of the normal stress peak is directly correlated with the yield stress of the material. Using three quantities: the lower bound fracture stress, (σ_{FLB}), as discussed in the preceding section (Fig. 10), the normal stress

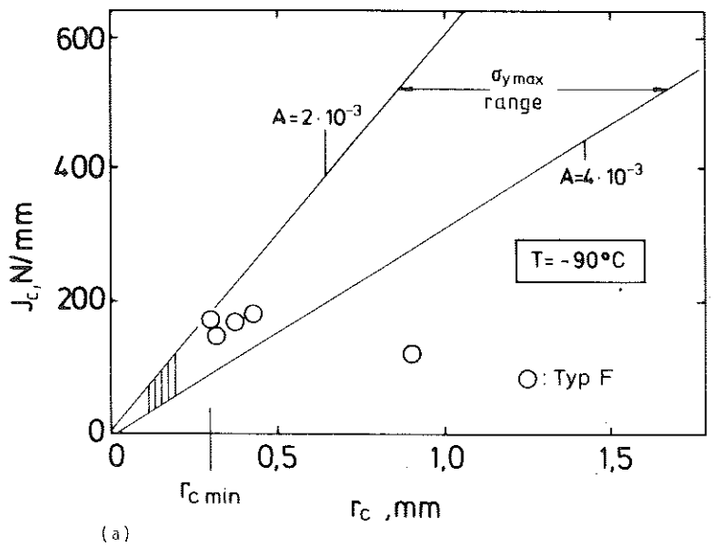

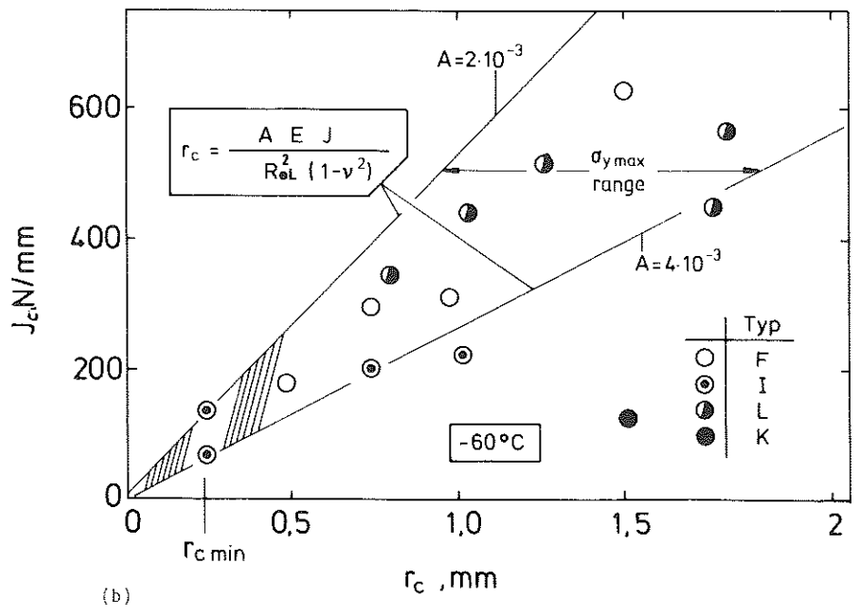

Fig 11 (a), (b) Relationship between the location of the initiation sites designated by r_c and the fracture toughness J_c. Lines indicate the approximate location of the normal stress peak in front of the crack tip: (a) at −90°C; (b) at −60°C

maximum as estimated with equation (2) using the value $A_m = 0.0027$ and the temperature dependence of the yield strength (Fig. 4), the RKR criterion leads to a definition of a transition temperature, called T_T. This temperature is characterized by the situation where the value of the stress peak is equal to the lower bound fracture stress

$$\sigma_{ymax} = \sigma_A \equiv \sigma_{FLB}$$

The result of this approach is shown in Fig. 12. The predicted transition temperature is in good agreement with the experimental results. Despite this obviously successful application of this model the main problem using this approach is the relatively low temperature dependence of the yield strength. This low temperature dependence of the yield strength has the consequence that small changes in the quantities used for the prediction lead to large variations in the predicted transition temperature. The hatched bar in Fig. 12 gives an impression how strong a very slight change of the yield strength or lower bound fracture stress influences the prediction.

The present work indicates that cleavage fracture behaviour of the specimen is strongly correlated to the normal stress peak at the crack tip. McMeeking and Parks **(12)** have investigated the influence of loading mode and ligament length on the normal stresses at a blunted crack tip by finite element calculations. Applying the model for the prediction of T_T as discussed above to the finite element calculations of reference **(12)** some conclusions concerning the transition behaviour of CCT (centre crack tension) – and ECB (edge crack

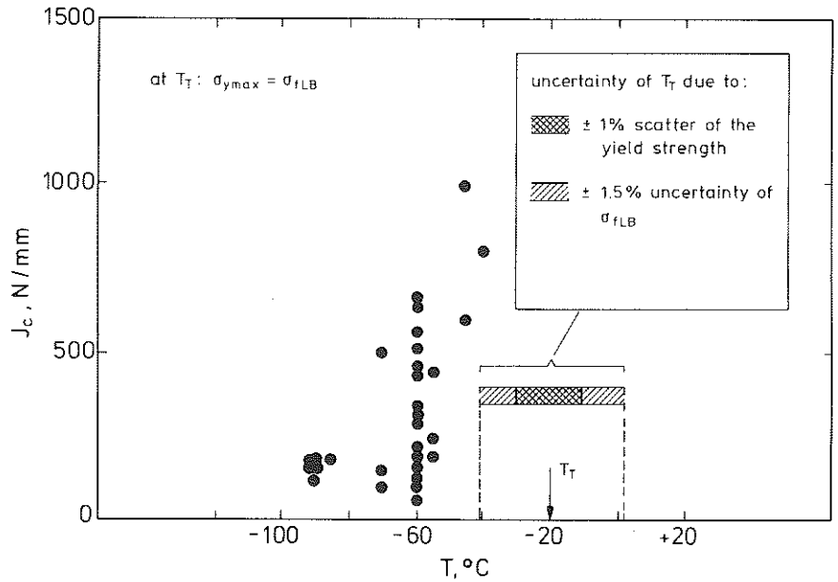

Fig 12 Estimation of the transition temperature T_T using the fracture criteria of Ritchie *et al.* (3)

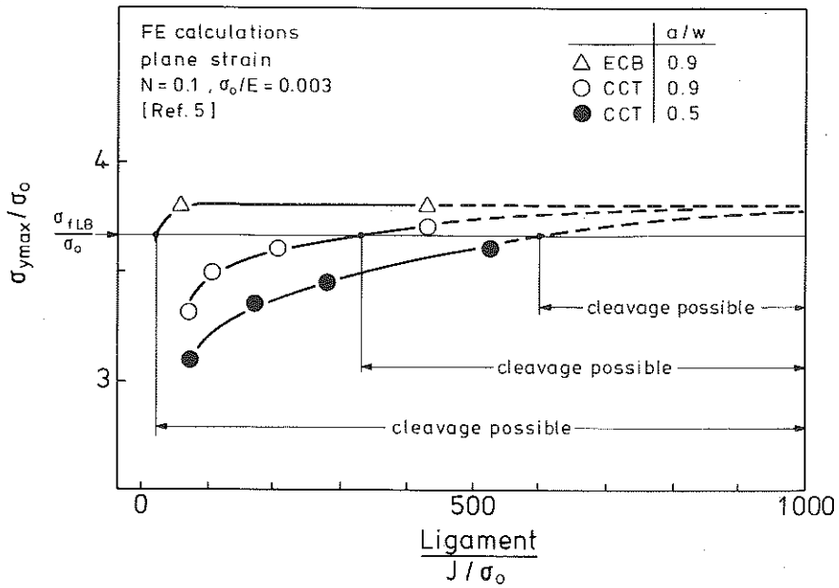

Fig 13 Behaviour of the normal stress peak under tension and bending load for plane strain taken from the numerical calculations of reference (12)

bending) – specimens can be drawn. As an extraction of the two dimensional plane strain finite element calculations the value of the normal stress peak as a function of both, the ligament length, L, and the J integral is shown in Fig. 13 (L is the width minus the crack length of the specimen.) It can be seen that there are substantial differences between the two types of specimens. With increasing J the maximum of the normal stress peak of a CCT specimen (tension loading) decreases steadily whereas for the ECB specimen (bending loading) the maximum of the stress peak stays constant up to $L\sigma_0/J = 25$. This means that even for a situation were the stress state does not change with increasing load the J integral does not have a size independent correlation to the normal stress peak. Using the findings of this paper which indicate that cleavage is cobtrolled by the normal stress peak, it can be concluded that the J integral is obviously not able to provide a geometry independent characterization of cleavage fracture. This means that the J integral is not an appropriate fracture parameter for cleavage fracture.

Conclusions

The fractographic results confirm that within the transition region cleavage fracture is triggered in one small volume in front of the fatigue crack tip that is the cleavage initiation site. This is in agreement with the 'weakest-link' hypotheses.

Four different types of cleavage initiation sites could be characterized. The type and the location of initiation site is influenced by the test temperature.

The initiation sites are located close to the maximum of the normal stresses in the ligament.

In the transition region a large part of the scatter of the fracture toughness J_c is due to the scatter of the distance between the crack tip and the initiation sites.

The fractographic results and the stress calculations confirm the RKR fracture criterion: In order to initiate cleavage fracture a 'critical stress' acting over a 'critical' distance must be reached or exceeded.

The RKR criterion was used to predict the transition temperature T_T.

According to the numerical calculations of McMeeking and Parks there is no specimen size independent correlation between the J integral and the normal stress in the ligament. Applying that result to the findings of the present paper it can be concluded that the J integral cannot provide a specimen size independent characterization of cleavage fracture.

Acknowledgements

The present work was part of a scientist exchange between the GKSS Research Centre and the National Institute of Standards and Technology (NIST) in Boulder, Colorado. The authors want to thank both organizations for supporting this exchange. The authors also express their appreciation to Dr H. McHenry for his very helpful discussions and suggestions.

References

(1) FAUCHER, B. and TYSON, W. R. (1988) A study of variability, size, and temperature effects on fracture toughness of an arctic-grade steel plate, *ASTM STP 945*, (Edited by D. T. Read and R. P. Reed), ASTM, Philadelphia, pp. 164–178.
(2) EHL, W., MUNZ, D., and BRÜCKNER, A. (1986) Scatter of the fracture toughness in the ductile to brittle transition region, *Proc. ECF6*, Amsterdam.
(3) RITCHIE, R. O., KNOTT, J. F., and RICE, J. F. (1973) On the relationship between critical tensile stress and fracture stress in mild steels, *J. Mech. Phys. Solids*, **21**, 395–410.
(4) ASTM E813-81 (1982) Standard method for J1c, a measure of fracture toughness, *ASTM-Standards*, Part 10, Metals.
(5) GRIFFITH, J. R. and OWEN, J. (1971) *J. Mech. Phys. Solids*, **19**, 491–431.
(6) HAHN, G. T. (1984) The influence of microstructure on brittle fracture toughness, *Metall. Trans*, **15A**, 947–959.
(6) CURRY, D. A. (1984) Influence of microstructure on yield stress and cleavage fracture stress at −196°C of SA508 class 2 pressure vessel steel, *Metal Science*, **18**, 67–76.
(7) McMAHON, C. J. and COHEN, M. (1965) *Acta Metall.*, **3**, 591–605.
(8) BROZZO, P., BUZZICHELLI, G., MASCANZONI, A. and MIRABELI, M. (1977) Microstructure and cleavage resistance of low carbon steel, *Metal Science*, **11**, 123–129.
(9) RITCHIE, R. O. and THOMPSON, A. W. (1985) On macroscopic and microscopic analysis for crack initiation and crack growth toughness in ductile alloys, *Metall. Trans.*, **15A**, 233–248.
(10) TRACY, D. M. (1976) Finite element solution for crack tip behaviour in small scale yielding, *J. Eng. Maths. Tech.*, **98**, 146–151.

(11) McMEEKING, R. M. (1977) Finite deformation analysis of crack tip opening in elastic–plastic materials and implication for fracture, *J. Mech. Solids*, **25**, 375–381.
(12) McMEEKING, R. M. and PARKS, D. M. (1979) Elast. Plast. Fracture, *ASTM STP 668* (Edited by J. D. Landes *et al.*), pp. 175–194.
(13) RICE, J. R. and JOHNSON, M. A. (1970) Inelastic behaviour of solids (Edited by M. F. Kanninen *et al.*), McGraw-Hill, pp. 641–672.
(14) SCHWALBE, K.-H. (1977) Comments to finite element solutions of crack-tip behaviour in small scale yielding, *Transactions of the ASM*, April, pp. 186–188.
(15) HEERENS, J. Rißabstumpfung, Spaltbruch im Übergangsbereich und stabiles Rißwachstum-Untersucht mit den Methoden der nichtlinearen Bruchmechanik, *GKSS-Report* in preparation.

DUCTILE FRACTURE DYNAMICS